Simulating two-qubit gates under the influence of charge defects in an FD-SOI device

Pericles Philippopoulos
Nanoacademic Technologies Inc.
Montreal, Canada
pericles@nanoacademic.com

Félix Beaudoin
Nanoacademic Technologies Inc.
Montreal, Canada
fbeaudoin@nanoacademic.com

Philippe Galy
STMicroelectronics
Crolles, France
philippe.galy@st.com

***Abstract*—The exchange interaction has been successfully used to mediate qubit entanglement in various semiconductor quantum devices. Using the finite-element method, we combine a nonlinear Poisson solver with single- and many-body Schrödinger solvers to simulate the exchange interaction between a pair of spin qubits in a fully depleted silicon-on-insulator (FD-SOI) device. We also modify the Poisson solver to account for charge impurities and evaluate the effect of a single impurity on the exchange interaction strength, including its dependence on the impurity's position. The effect of the impurity on the exchange strength is then analyzed to calculate the average two-qubit gate fidelity achievable via the exchange interaction when the system is subject to charge noise arising from a charge randomly tunneling in and out of an interface impurity trap. The presented approach demonstrates the possibility of simulating key quantum-device performance metrics, such as two-qubit gate fidelity, starting only from the device geometry.**

***Index Terms*—FD-SOI, two-qubit gate, exchange, charge noise**

I. Introduction

Due to their compatibility with industrial semiconductor fabrication processes, electron spins confined to silicon quantum dots have emerged as a main qubit candidate in scalable quantum information technologies [1]. Because quantum systems operate based on principles that are not applicable to classical systems (e.g. superposition, entanglement), specialized (TCAD) tools are required to simulate these systems. In this work, we developed such a tool to understand tunneling and exchange of electrons confined to neighboring quantum dots, within the `Quantum Technology Computed-Aided Design` (QTCAD®) framework [2]–[5]. We apply this tool to a model fully depleted silicon-on-insulator (FD-SOI) double-dot device, inspired by STMicroelectronics standard fabrication processes, but with dimensions comparable to state-of-the-art two-qubit MOS devices [6] (see Fig. 1). Moreover, we explore how charge noise in the form of a fluctuating point-charge defect at the Si/SiO_2 interface can affect the fidelity of a quantum two-qubit gate implemented using the exchange interaction.

This work is supported by the Chips JU project ARCTIC (Project #101139908). The project is supported by the Chips Joint Undertaking and its members (including top-up funding by Belgium, Austria, Germany, Estonia, Finland, France, Ireland, The Netherlands and Sweden). ARCTIC gratefully acknowledges the support of the Canadian and the Swiss federal governments.

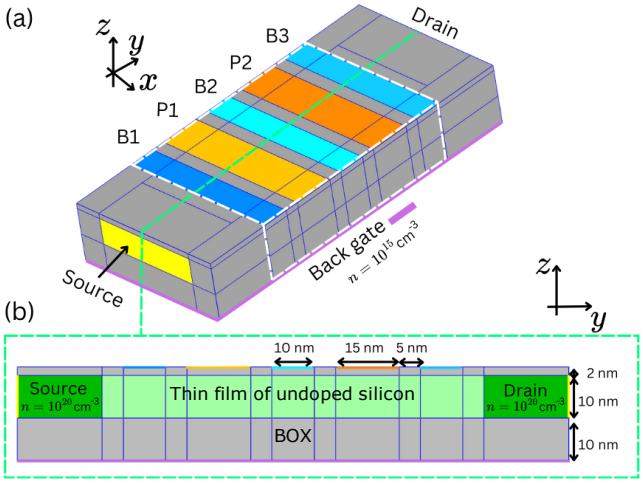

Fig. 1. Double-dot FD-SOI device inspired by STMicroelectronics' standard fabrication processes. (a) 3D model of the device. (b) Cut in the yz plane along the green dashed line. Five top gates, two plunger gates (orange surfaces), P1 and P2, and three barrier gates, B1, B2, and B3 (blue surfaces) provide tunability for confinement and tunneling respectively. Notably, gate B2 is used to control the interdot tunneling. A thin layer (2 nm) of SiO_2 separates the gates from the undoped silicon channel (mint green region) where a double-dot confinement potential is formed for suitable applied voltages to the top gates, one dot below each plunger gate. Doped source and drain regions with $n = 10^{20}\,\mathrm{cm}^{-3}$ (dark green region) act as electron reservoirs and Ohmic contacts enforce charge-neutral equilibrium across the identified boundaries (yellow surfaces). The rest of the device is SiO_2 (gray regions). The device is also equipped with a back gate (purple boundary) separated from the channel by a buried oxide layer (BOX, 10 nm) which is used to put the bottom of the structure at equilibrium with the rest of the substrate which has background doping of $n = 10^{15}\,\mathrm{cm}^{-3}$. The width of the channel along the x direction is 40 nm.

II. Poisson and Schrödinger solvers

A model of the device we investigate is depicted in Fig. 1. We generate a finite-element mesh over this model to discretize the equations we solve and start the simulation workflow by solving the nonlinear Poisson equation which relates the electric potential $\varphi(\mathbf{r})$ to the charge density $\rho[\varphi]$

$$-\nabla \cdot [\varepsilon(\mathbf{r})\nabla\varphi(\mathbf{r})] = \rho[\varphi], \tag{1}$$

where $\varepsilon(\mathbf{r})$ is the electric permittivity. Additionally, the potential $\varphi(\mathbf{r})$ is subject to the boundary conditions

$$\varphi(\mathbf{r}) = \varphi_i \quad \forall \mathbf{r} \in \Sigma_i, \tag{2}$$

where i runs over the eight gates/contacts depicted in Fig. 1 (the plunger gates P1 and P2, the barrier gates B1, B2, and B3, the back gate, and the source and drain Ohmic contacts) and φ_i is the value of the potential at the surface Σ_i which is enforced by the device gates/contacts [nongray surfaces in Fig. 1 (a)]. In (1), the charge density is computed by filling parabolic bands according to the Fermi-Dirac distribution, except in the channel below the top gates [outlined with the white dashed line in Fig. 1 (a)] where quantized charges are expected to be located. In this region, the charge density $\rho[\varphi]$ is set to zero. We solve the nonlinear Poisson equation at a constant cryogenic temperature [7], $T = 100\,\mathrm{mK}$, where we expect the device to operate. At low temperatures, $\rho[\varphi]$ depends exponentially on φ, leading to convergence issues which are circumvented using adaptive meshing [3].

For a range of voltages V_{B2} applied to the barrier gate B2, we solve the nonlinear Poisson equation to obtain $\varphi(\mathbf{r})$ and the associated confinement potential $V(\mathbf{r})$ (given by the conduction-band edge). The confinement potential is input into the single-particle Schrödinger equation, which is solved under the effective-mass approximation for a single z-valley, to obtain eigenfunctions $\psi_i(\mathbf{r})$ and eigenenergies ϵ_i. For each V_{B2}, we tune the system to the symmetric configuration (by adjusting the plunger-gate voltages), characterized by the electron being equally distributed between both dots and the energy splitting Ω between the (delocalized) ground and the first-excited states being minimal (see Fig. 2). In this configuration, $\Omega = 2t_c$, where t_c/h represents the tunneling rate between the dots, and h is Planck's constant. Therefore, by minimizing Ω with respect to the plunger-gate detuning, we can compute t_c.

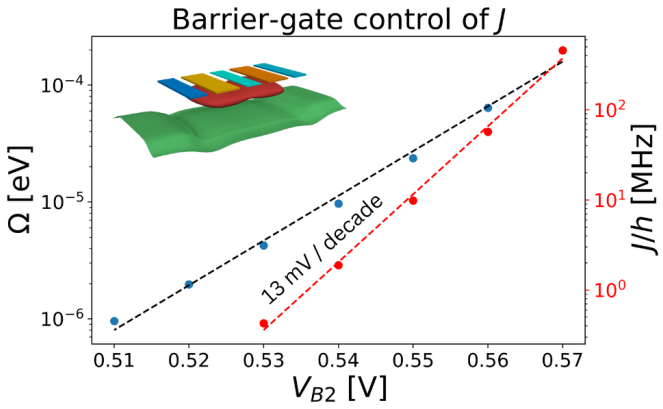

Fig. 2. Energy splitting, Ω, of the ground and first-excited states in the symmetric configuration of the double-dot system depicted in Fig. 1, as a function of V_{B2}. The exchange frequency, J/h, versus V_{B2} is plotted in red. Inset: Equipotential surface (green) and equiprobability surface of the ground-state wavefunction (red) for $V_{B2} = 0.57\,\mathrm{V}$ in the symmetric configuration, showing the electron shared between both dots. The colors of the rectangular gates match those in Fig. 1.

III. Exchange Calculation

Two-qubit gates have been demonstrated in (silicon-based) MOS devices using the exchange interaction between neighboring dots [6], [8]. The exchange Hamiltonian, which generates this interaction, is given by $H_J = J\mathbf{S}_1\cdot\mathbf{S}_2$, where J is the strength of the interaction and $\mathbf{S}_i$ is the spin of the electron in dot i. Exchange is a consequence of the Pauli exclusion principle and can be derived by solving a quantum many-body Hamiltonian. In particular, J is given by the energy splitting between the spin singlet and triplet states Δ_{ST} in a system of two electrons, i.e., $J = \Delta_{ST}$. Accordingly, we construct the many-body Hamiltonian accounting for Coulomb interactions between electrons in the two-electron subspace, using (28 spin-degenerate, i.e. 56) single-particle orbitals $\psi_i(\mathbf{r})$ (computed by diagonalizing the single-body Hamiltonian, see section II) as a basis. This Hamiltonian is diagonalized to extract $J = \Delta_{ST}$. Fig. 2 demonstrates how J can be tuned by several orders of magnitude using the voltage applied to B2, V_{B2}.

IV. Interface Charge

Next, we investigate how J is affected by a charge impurity located at the interface between the silicon channel and the oxide that separates it from the gates. This impurity can be thought of as an electron (or hole) tunneling in and out of an interface impurity trap and is modeled using a Gaussian charge-density profile spread over a radius $\sigma = 1\,\text{Å}$ with total charge $q = \pm e$. Because σ is much smaller than the dimensions of the device, we consider the impurity to be a point charge. The associated charge density is given by

$$\rho_{\mathbf{R}}(\mathbf{r}) = \frac{q}{(2\pi)^3\sigma^3} e^{-\frac{(\mathbf{r}-\mathbf{R})^2}{2\sigma^2}}, \tag{3}$$

where $\mathbf{R}$ is the position of the charge trap/impurity.

Including this charge density on the right-hand side of (1) leads to screening of $\rho_{\mathbf{R}}(\mathbf{r})$ by the (continuous) charge density $\rho[\varphi]$. Therefore, to account for this extra charge, a modified version of the Poisson equation is solved. First, as in the impurity-free case described above, we solve the nonlinear Poisson equation subject to the boundary conditions of (2). Then, we also solve the linear Poisson equation $-\nabla\cdot[\varepsilon(\mathbf{r})\nabla\varphi_{\mathbf{R}}(\mathbf{r})] = \rho_{\mathbf{R}}(\mathbf{r})$, accounting only for the point charge, and enforce the boundary conditions

$$\varphi_{\mathbf{R}}(\mathbf{r}) = 0 \quad \forall \mathbf{r} \in \bigcup_{i=1}^{8} \Sigma_i. \tag{4}$$

The full solution for an impurity at position $\mathbf{R}$ is taken to be $\varphi(\mathbf{r}) + \varphi_{\mathbf{R}}(\mathbf{r})$.

To properly capture the features of the point charge, it is necessary to construct a well-suited finite-element mesh. In addition to the adaptive meshing required to converge the nonlinear Poisson equation at cryogenic temperatures, to resolve the features of the impurity, the characteristic length of the mesh near the impurity is forced to be $\sigma/5$. The meshes used in the simulations presented here contain $\sim 8\times10^5$ nodes.

We place a single point charge at various locations at the Si/SiO_2 interface (near the gates P1, B2, and P2) and solve the Poisson equation to obtain the confinement potential $V(\mathbf{r})$ (see Fig. 3). Then, the many-body Hamiltonian is diagonalized to map out the exchange as a function of charge-impurity

position [see Fig. 4 (a) and (b)]. In this case, to limit the computational resources used during the simulations, we used a basis comprised of 16 spin-degenerate single-particle orbitals. This number of orbitals led to values of exchange that are within 1% of the values presented in Fig. 2 (computed with 28 spin-degenerate single-particle orbitals) in the impurity-free calculation.

Since J is a consequence of the Coulomb interaction, it increases as the distance between electrons decreases. With this in mind, we can understand the qualitative features of the results displayed in Figs. 4 (a) and (b). For example, for a charge $q = \pm e$ positioned between the two dots, near gate B2, the exchange increases (decreases) with respect to the impurity-free value, since the positive (negative) point charge attracts (repels) the electrons in the dots toward (away from) each other.

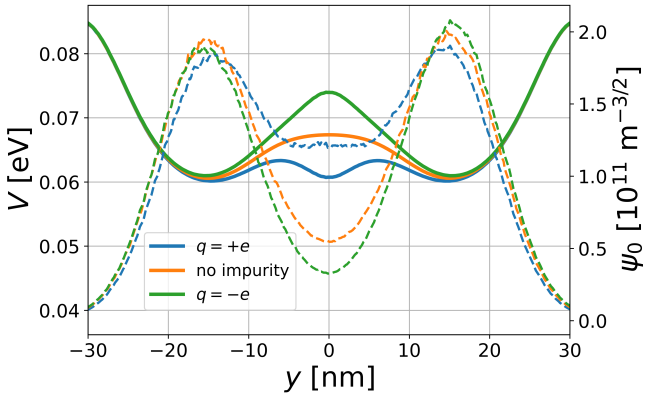

Fig. 3. Linecuts of the confinement potential $V(\mathbf{r})$ (solid lines, left axis) and ground-state single-particle wavefunction $\psi_0(\mathbf{r})$ (dashed lines, right axis). The linecuts are taken through the center of the channel. The plunger gates (between $\pm 10\,\mathrm{nm}$ and $\pm 25\,\mathrm{nm}$) create a double-well potential. The results for an impurity with charge $q = \pm e$ positioned at the center of B2, $y = 0\,\mathrm{nm}$, at the Si/SiO_2 interface are plotted in blue (green). The results in the absence of a charge impurity are plotted in orange. When $q = \pm e$, the potential under B2 is suppressed (increased) relative to the impurity-free case leading to a larger (smaller) probability of the electron occupying the region between both dots and consequently a larger (smaller) value for J.

V. Two-Qubit Gate Fidelities

A. Dynamics under the exchange Hamiltonian

Before analyzing two-qubit gate fidelities, we start by considering the dynamics of a two-qubit system under the influence of the exchange interaction. We consider the following basis for the two-qubit states: $|s_1 s_2\rangle \in \{|\uparrow\uparrow\rangle, |\uparrow\downarrow\rangle, |\downarrow\uparrow\rangle, |\downarrow\downarrow\rangle\}$, where s_1 (s_2) is the spin state of the first (second) qubit. In this basis, the exchange Hamiltonian can be written as

$$H_J = J\mathbf{S}_1 \cdot \mathbf{S}_2 = \frac{J}{4} - \frac{J}{2}\mathbb{I} + \frac{J}{2}\sigma_x, \tag{5}$$

where $\mathbb{I} = |\uparrow\downarrow\rangle\langle\uparrow\downarrow| + |\downarrow\uparrow\rangle\langle\downarrow\uparrow|$ and $\sigma_x = |\uparrow\downarrow\rangle\langle\downarrow\uparrow| + |\downarrow\uparrow\rangle\langle\uparrow\downarrow|$. Therefore, H_J acts trivially on the polarized triplet states $|\uparrow\uparrow\rangle$ and $|\downarrow\downarrow\rangle$. Accordingly, we neglect these and focus on the exchange Hamiltonian projected onto the subspace spanned by the remaining states, i.e., $\bar{H}_J = -\frac{J}{4}\mathbb{I} + \frac{J}{2}\sigma_x$. Because the first term in $\bar{H}_J$ does not induce any nontrivial dynamics, we can further limit ourselves to considering only $\frac{J}{2}\sigma_x = \frac{\hbar}{2}\mathbf{\Omega}_J \cdot \boldsymbol{\sigma}$, where $\mathbf{\Omega}_J = [J/\hbar, 0, 0]$ is the angular frequency vector associated with $\bar{H}_J$ and $\boldsymbol{\sigma} = [\sigma_x, \sigma_y, \sigma_z]$ is the vector of Pauli matrices with $\sigma_z = |\uparrow\downarrow\rangle\langle\uparrow\downarrow| - |\downarrow\uparrow\rangle\langle\downarrow\uparrow|$ and $\sigma_y = \frac{1}{2i}[\sigma_z, \sigma_x]$.

For a pure state $|\psi\rangle$ (in a two-dimensional Hilbert space), the density matrix can be written as $\varrho = |\psi\rangle\langle\psi| = \frac{1}{2}(\mathbb{I} + \mathbf{M} \cdot \boldsymbol{\sigma})$, which defines an effective magnetization vector $\mathbf{M}$. The dynamics of this vector are given by the Bloch equations $\dot{\mathbf{M}}(t) = \mathbf{\Omega}_J \times \mathbf{M}(t)$ [9]. Because $\mathbf{\Omega}_J$ has vanishing y and z components, M_x will be constant in time. For an initial state $|\psi_0\rangle = |\uparrow\downarrow\rangle$ we find $M_-(t) \equiv M_z(t) - iM_y(t) = e^{i\Omega_J t}$. If the system evolves for a time $\tau = \frac{\pi}{\Omega_J}$, then $M_-(\tau) = -1$, or equivalently, the final state of the system will be $|\psi_f\rangle = \exp[-i\mathbf{\Omega}_J \cdot \boldsymbol{\sigma}\tau]|\uparrow\downarrow\rangle = |\downarrow\uparrow\rangle$. The effect of the operator SWAP $\equiv \exp[-i\mathbf{\Omega}_J \cdot \boldsymbol{\sigma}\tau]$ is therefore to "swap" the states of the qubits. However, this gate does not generate entanglement. In contrast, $\sqrt{\mathrm{SWAP}} \equiv \exp\left[-i\frac{\pi}{2}\sigma_x\right]$, which is implemented by allowing the system to evolve under the exchange Hamiltonian for a time $\tau/2$, does generate entanglement. We will therefore focus on the fidelity of the $\sqrt{\mathrm{SWAP}}$ gate below.

B. Dynamics under the influence of a single fluctuator

In the absence of all impurities, applying $\sqrt{\mathrm{SWAP}}$ to the two-qubit system described above would involve initializing the system in the state $|\psi_0\rangle$, applying a sufficiently high voltage to gate B2 to generate a constant exchange Hamiltonian H_J, and allowing unitary evolution of the system for a time $\tau/2 = \frac{\pi}{2\Omega_J}$. In the presence of charge noise in the form of a fluctuating interface charge impurity, the exchange energy becomes time dependent, $J(t) = J_0 + \delta J\chi(t)$, where $J_0 \pm \delta J$ is the exchange energy in the absence (presence) of the impurity and $\chi(t)$ is a random signal that jumps between 1 and -1 with an average switching rate γ. If the jumps of the random signal are exponentially distributed so that the number of fluctuations in a given time are Poisson distributed, we can use the results of [9] to write an analytic expression for the average dynamics of $M_-(t)$ under the influence of the fluctuator. For $M_-(0) = 1$, which corresponds to the initial state $|\psi_0\rangle = |\uparrow\downarrow\rangle$,

$$\langle M_-(t)\rangle = e^{iJ_0 t/\hbar - \gamma t}\left[\cos(\omega t) + \frac{\gamma}{\omega}\sin(\omega t)\right], \tag{6}$$

where $\omega = \sqrt{(\delta J/\hbar)^2 - \gamma^2}$.

C. $\sqrt{\mathrm{SWAP}}$ gate fidelities

Using (6) we can compute the average density matrix of the two-qubit system under the influence of a single fluctuator, $\bar{\varrho}(t) = \frac{1}{2}(\mathbb{I} + \langle\mathbf{M}(t)\rangle \cdot \boldsymbol{\sigma})$. Here, $\langle\mathbf{M}_x(t)\rangle = 0$, $\langle\mathbf{M}_y(t)\rangle = -\mathrm{Im}[\langle M_-(t)\rangle]$, and $\langle\mathbf{M}_z(t)\rangle = \mathrm{Re}[\langle M_-(t)\rangle]$. The average $\sqrt{\mathrm{SWAP}}$ fidelity implemented with the exchange interaction becomes $\bar{F}(t) = \langle\psi_0|\sqrt{\mathrm{SWAP}}^\dagger \bar{\varrho}(t)\sqrt{\mathrm{SWAP}}|\psi_0\rangle$, where $|\psi_0\rangle$ is the initial state of the system. For $|\psi_0\rangle = |\uparrow\downarrow\rangle$ the average fidelity takes the following analytic form

$$\bar{F}(t) = \frac{1}{2} + \frac{1}{2}\mathrm{Im}\left\{e^{iJ_0 t/\hbar - \gamma t}\left[\cos(\omega t) + \frac{\gamma}{\omega}\sin(\omega t)\right]\right\}, \tag{7}$$

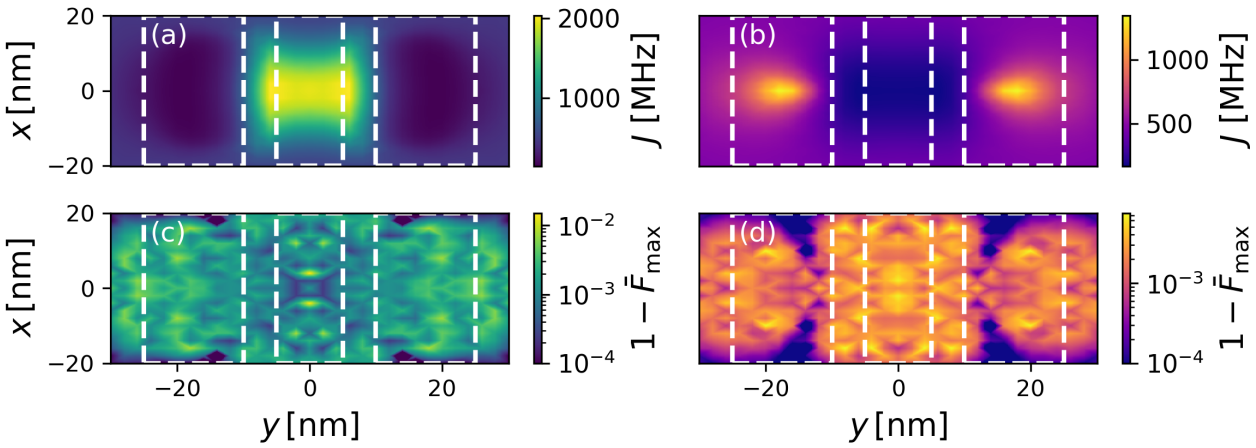

Fig. 4. Exchange energy J and minimal average error on fidelity $1-\bar{F}_{\max}$ (color scales), computed as a function of the position of a single charge impurity located at the interface between the silicon channel and the oxide that separates it from the gates. The first column of subplots corresponds to $q=+e$, while the second column corresponds to $q=-e$. The exchange energy J is shown in (a) and (b) for $q=+e$ and $q=-e$ respectively. The minimal average error on fidelity $1-\bar{F}_{\max}$ is computed using Eq. (7) and plotted for $\gamma=10^5$ Hz in (c) and (d). The dashed white lines correspond to the outline of the gates P1, B2, and P2. The barrier-gate bias is set to $V_{B2}=0.57\,\mathrm{V}$. The minimal average errors [Figs. (c)-(d)] are capped at the lower bounds for the respective color scales such that any error below the lower bound is represented by the color of the lower bound (i.e. purple).

In our simulations, we consider $\gamma=10^5$ Hz. This frequency is within the range that was probed in [10] using dynamical decoupling in FD-SOI spin-qubit devices at a temperature similar to that used in our simulations, $T=120\,\mathrm{mK}$. Importantly, the noise power spectral density in these devices was found to be well described by a $1/f$ fit, which is a signature of charge noise induced by two-level fluctuators. Therefore, the experiments of [10] provide evidence that two-level fluctuators are an important source of noise to consider in these types of devices.

For each impurity position and charge $q=\pm e$, we compute the maximal average fidelity $\bar{F}_{\max}=\max_t \bar{F}(t)$. The results are displayed in Fig. 4. We find minimal errors on the fidelity $1-\bar{F}_{\max}$ that differ by orders of magnitude depending on the sign and position of the interface charge defect. Moreover, there are regions at the interface where the presence of charge impurities would prevent the fidelity from achieving state-of-the-art values, $\gtrsim 99\%$ [6].

VI. Conclusion

Using a specialized (TCAD) simulation tool designed specifically for quantum systems, we are able to investigate the behavior of a model FD-SOI double-dot device at cryogenic temperatures. Access to the many-body energies has allowed us to make quantitative predictions about the possible values of exchange in this device and to simulate realistic two-qubit gates in this system under the influence of a fluctuating interface charge defect. We can identify defect locations that lead to errors orders of magnitude worse than others which can help target efforts to improve next-generation devices. Moreover, the qualitative difference between the interface map (Fig. 4) for defects with $q=+e$ and $q=-e$ can be used in conjunction with measurements to determine the sign of fluctuating interface charge defects in these types of devices.

The gate fidelities simulated here are assumed to be limited by charge noise which is modeled as arising from a single point charge tunneling in and out of an interface trap. In practice, the number of interface impurities is characterized by a density of interface traps (DIT). A natural extension of this work would therefore be to incorporate multiple impurities, randomly positioned according to a realistic DIT. Nonetheless, the framework presented here showcases the capability of existing simulation tools to predict key quantum device performance metrics, such as two-qubit gate fidelities, using only device geometries.

References

[1] T. Meunier, N. Daval, F. Perruchot, and M. Vinet. Silicon spin qubits: a viable path towards industrial manufacturing of large-scale quantum processors. *Eur. Phys. J. A*, 61(58), 2025.

[2] https://nanoacademic.com/solutions/qtcad/.

[3] F. Beaudoin et al. Robust technology computer-aided design of gated quantum dots at cryogenic temperature. *Appl. Phys. Lett.*, 120(26):264001, 2022.

[4] R. J. Prentki et al. Robust sub-Kelvin simulations of quantum dot charge sensing. In *2023 International Conference on Simulation of Semiconductor Processes and Devices (SISPAD)*, pages 349–352. IEEE, 2023.

[5] P. Philippopoulos, F. Beaudoin, and P. Galy. Analysis and 3D TCAD simulations of single-qubit control in an industrially-compatible FD-SOI device. *Solid-State Electronics*, 215:108883, 2023.

[6] T. Tanttu et al. Assessment of the errors of high-fidelity two-qubit gates in silicon quantum dots. *Nat. Phys.*, 20:1804–1809, 2024.

[7] P. Galy et al. Cryogenic temperature characterization of a 28-nm FD-SOI dedicated structure for advanced CMOS and quantum technologies co-integration. *IEEE Journal of the Electron Devices Society*, 6:594–600, 2018.

[8] M. Veldhorst et al. A two-qubit logic gate in silicon. *Nature*, 526:410–414, 2015.

[9] J. Bergli, Y. M. Galperin, and B. L. Altshuler. Decoherence in qubits due to low-frequency noise. *New J. Phys.*, 11(025002), 2009.

[10] B. Klemt et al. Electrical manipulation of a single electron spin in CMOS using a micromagnet and spin-valley coupling. *npj Quantum Inf*, 9(107), 2023.